A posteriori analysis of a dynamic nonequilibrium model for subfilter scalar variance and dissipation rate

By C. M. Kaul AND V. Raman

1. Motivation and objectives

Subfilter scalar variance and subfilter scalar dissipation rate are key quantities used to characterize the small-scale, unresolved scalar mixing process in large eddy simulation (LES) of nonpremixed combustion. Together or singly, these two quantities are important inputs to a number of LES combustion modeling approaches that employ mixture fraction-based parameterizations. Despite the practical importance of scalar variance and dissipation rate modeling, a significant weakness can be identified in each of the two main modeling strategies in widespread use. Models following the first of these strategies can be categorized as equilibrium models because they rely on the assumption that rates of variance production and dissipation are locally in balance (Pierce & Moin 1998). While the validity of the equilibrium assumption for even the simplest turbulent flows has been disputed (da Silva & Pereira 2005), these models remain popular because they can be combined with dynamic procedures (Pierce & Moin 1998; Balarac *et al.* 2008) to provide all required model coefficients. The second category of models, referred to as nonequilibrium models, solve a transport equation for variance (Jimenez *et al.* 2001) and thus offer a more complete description of small scale mixing that does not (in fact, cannot) invoke a local balance between production and dissipation. Instead, an explicit model for the subfilter scalar dissipation rate is required. Most commonly, this dissipation rate model has taken the form of an algebraic expression multiplied by a flow-dependent model coefficient, denoted here as $\mathcal{C}_\tau$. A satisfactory dynamic procedure for estimating this model coefficient has not previously been available, making it necessary to set $\mathcal{C}_\tau$ to some assumed value. This modeling practice is clearly undesirable when LES is used in a predictive manner, without the benefit of any reference data that can be used to tune the coefficient value.

Recently, an alternative form of dynamic procedure was used to determine $\mathcal{C}_\tau$ in LES of a lifted, auto-igniting turbulent ethylene flame (Kaul *et al.* 2012). While this study demonstrated the usefulness of the model for LES of practical relevance, definitive conclusions about the accuracy of its $\mathcal{C}_\tau$ predictions could not be made. It was instead recognized that the new dynamic procedure for $\mathcal{C}_\tau$ should not be viewed simply as a modeling add-on to existing nonequilibrium models. Instead, the variance transport equation, scalar dissipation rate closure, and $\mathcal{C}_\tau$ estimate are tightly linked and together form a dynamic nonequilibrium model for scalar variance and scalar dissipation rate. Additionally, the lifted flame simulation, like the overwhelming majority of LES computations, used grid-based filtering, which is known to make LES results, including variance model predictions, prone to large numerical errors (see Kaul *et al.* (2009) , Kaul & Raman (2011), and references therein). This numerical error further complicated a posteriori analysis of the dynamic nonequilibrium model's performance.

Here, a technique called the coupled DNS-LES method (Kaul & Raman 2011), which was specifically developed for a posteriori analysis of LES scalar modeling, is used to examine how the variance transport equation, scalar dissipation rate closure, and $\mathcal{C}_\tau$ dynamic procedure function together as a dynamic nonequilibrium model describing subfilter scalar mixing. The use of the coupled DNS-LES method greatly clarifies the model analysis by removing the effects of finite difference and turbulence modeling errors. Nonetheless, understanding the sources of error in the model's predictions in three-dimensional turbulence remains challenging. Therefore, a third level is added to the model analysis hierarchy of full LES and coupled DNS-LES by developing a "model of the model" based on the time-dependent ordinary differential equation describing the evolution of the volume-averaged variance. This representation of the mean scalar variance evolution, albeit an abstraction and simplification of the actual model, adds further insight into how the dynamically predicted values of $\mathcal{C}_\tau$ modulate or amplify errors in other terms of the dynamic nonequilibrium model.

2. Modeling background

A brief discussion of nonequilibrium variance modeling only is provided here. A more comprehensive overview of variance modeling can be found in Kaul *et al.* (2009) or Kaul & Raman (2011), while Pitsch (2006) reviews LES combustion modeling in general.

Models for nonpremixed combustion typically use a scalar variable called the mixture fraction, denoted here by Z, to parameterize mixture composition. In LES of a gas-phase system, the transport equation for the filtered mixture fraction can be written as

$$\frac{\partial \overline{\rho}\widetilde{Z}}{\partial t} + \frac{\partial \overline{\rho}\tilde{u}_i\widetilde{Z}}{\partial x_i} = \frac{\partial}{\partial x_i}\left[\overline{\rho}\left(D + D_T\right)\frac{\partial \widetilde{Z}}{\partial x_i}\right]. \tag{2.1}$$

In Eq. (2.1), $\overline{\rho}$ denotes the filtered density, $\tilde{u}_i$ denotes the i-th filtered velocity component, and D denotes the molecular diffusivity. The quantity D_T is the turbulent diffusivity appearing in the gradient diffusion closure for the subfilter scalar flux. The operator $\overline{(\cdot)}$ is a low pass spatial filtering operation characterized by a filterwidth Δ (Pope 2000). This spatial filter is used to define the density-weighted, or Favre, filtering operation $\widetilde{(\cdot)}$. Specifically, the Favre filtered mixture fraction is given by $\widetilde{Z} = \overline{\rho Z}/\overline{\rho}$. The $\overline{(\cdot)}$ and $\widetilde{(\cdot)}$ operators are equivalent for a flow with constant, uniform density (such as the one simulated in this study). For generality, however, all flow equations will be provided in terms of the Favre filtering operator.

Presumed probability density function closures for the subfilter distribution of mixture fraction require the subfilter scalar variance,

$$Z_v = \widetilde{Z^2} - \widetilde{Z}^2, \tag{2.2}$$

as an input. A transport equation for Z_v can be developed through purely mathematical manipulation of the mixture fraction transport equation. Once subfilter flux terms have been closed, the variance transport equation (VTE) model (Jimenez *et al.* 2001) takes the form

$$\frac{\partial \overline{\rho}Z_v}{\partial t} + \frac{\partial \overline{\rho}\tilde{u}_i Z_v}{\partial x_i} = \frac{\partial}{\partial x_i}\left[\overline{\rho}\left(D + D_T\right)\frac{\partial Z_v}{\partial x_i}\right] + 2\overline{\rho}D_T\frac{\partial \widetilde{Z}}{\partial x_i}\frac{\partial \widetilde{Z}}{\partial x_i} - \overline{\rho}\widetilde{\epsilon_Z}. \tag{2.3}$$

The second term on the right-hand side of Eq. (2.3) is associated with the production of variance and will be referred to by the notation $\mathcal{P}$. It should be noted, however, that

the production term in its unclosed, exact form can actually have a negative value due to misalignment of the subfilter scalar flux and filtered scalar gradient.

The quantity $\widetilde{\epsilon}_Z$ appearing in Eq. (2.3) is the subfilter scalar dissipation rate,

$$\widetilde{\epsilon}_Z = 2D\widetilde{\frac{\partial Z}{\partial x_i}\frac{\partial Z}{\partial x_i}} - 2D\frac{\partial \widetilde{Z}}{\partial x_i}\frac{\partial \widetilde{Z}}{\partial x_i}, \tag{2.4}$$

which is simply the difference between the filtered scalar dissipation rate $\widetilde{\chi}_Z$ [the first term on the right-hand side of Eq. (2.4)] and the resolved scalar dissipation rate [the second term on the right-hand side of Eq. (2.4)]. A model for either $\widetilde{\chi}_Z$ or $\widetilde{\epsilon}_Z$ suffices to model both quantities, because the resolved dissipation can be computed from the filtered mixture fraction solution.

While a transport equation model for $\widetilde{\chi}_Z$ has been formulated (Knudsen *et al.* 2012), it is more common to use an algebraic expression

$$\widetilde{\epsilon}_Z = \mathcal{C}_\tau \frac{Z_v}{\tau_Z} \tag{2.5}$$

to model the scalar dissipation rate. In Eq. (2.5), $\mathcal{C}_\tau$ is the model coefficient referred to in Section 1 and τ_Z is a mixing timescale (Peters 2000). Of the several different expressions for τ_Z, the common closure

$$\tau_Z = \frac{\Delta^2}{D + D_T} \tag{2.6}$$

is used here (Raman & Pitsch 2006).

While Eq. (2.5) appears extremely simple, it has interesting implications. The exact quantity $\widetilde{\epsilon}_Z$, as defined by Eq. (2.4), depends on the smallest scales of scalar turbulence, which are generally much smaller than the LES filterwidth. This is why the usual approach to setting up a dynamic modeling procedure [pioneered by Germano *et al.* (1991) and subsequently used for model development by Moin *et al.* (1991) and Pierce & Moin (1998), among others] is not useful for modeling dissipation rates; sub-testfilter and subfilter dissipation values are both dependent on the same small length scales. However, the model provided by Eq. (2.5) and Eq. (2.6) relates the subfilter scalar dissipation to the variance and eddy diffusivity, which, while also subfilter quantities, are determined by near-filterwidth scales of turbulence. Thus, it becomes possible to estimate $\mathcal{C}_\tau$ dynamically in terms of the expression $\mathcal{C}_\tau Z_v/\tau_Z$ once it has been substituted into the variance transport equation model, Eq. (2.3). This alternative basis for dynamic modeling was developed by Ghosal *et al.* (1995) for closure of the dissipation term in a subfilter kinetic energy transport equation model. However, it should be noted that a different, novel method is used here and in Kaul *et al.* (2012) for actually evaluating the model coefficient $\mathcal{C}_\tau$ to provide a robust, as well as accurate, estimate.

3. Coefficient estimation procedure

The first step to formulating a dynamic procedure for $\mathcal{C}_\tau$ is to recognize that the variance transport equation can be applied at both the filter scale Δ and a somewhat larger test-filter scale $\widehat{\Delta}$, which is usually equal to 2Δ. The spatial test-filtering operation is indicated by $\widehat{(\cdot)}$ and can be used to form a test-filter scale Favre filter operator $\widetilde{(\cdot)}$,

$$\breve{Z} = \frac{\widehat{\overline{\rho}\overline{Z}}}{\widehat{\overline{\rho}}} = \frac{\widehat{\overline{\rho}\widetilde{Z}}}{\widehat{\overline{\rho}}}. \tag{3.1}$$

With this notation for the test-filtering operations, the transport equation for the subtestfilter scalar variance, defined as $Z_t = \widetilde{\breve{Z}\breve{Z}} - \breve{\tilde{Z}}\breve{\tilde{Z}}$, can be written in analogy to the subfilter variance transport equation [Eq. (2.3)] as

$$\frac{\partial \hat{\overline{\rho}} Z_t}{\partial t} + \frac{\partial \hat{\overline{\rho}} \breve{u}_i Z_t}{\partial x_i} = \frac{\partial}{\partial x_i}\left[\hat{\overline{\rho}}\left(D + D_T^t\right)\frac{\partial Z_t}{\partial x_i}\right] + 2\hat{\overline{\rho}} D_T^t \frac{\partial \breve{\tilde{Z}}}{\partial x_i}\frac{\partial \breve{\tilde{Z}}}{\partial x_i} - \mathcal{C}_\tau \hat{\overline{\rho}}\frac{Z_t}{\tau_Z^t}. \tag{3.2}$$

In Eq. (3.2), a superscript t indicates a model quantity evaluated at the test-filter level (e.g., D_T^t) rather than a test-filtered subfilter model quantity (e.g., $\widehat{D_T}$). Note that it has been assumed that $\mathcal{C}_\tau$ has the same value at both filter scales. Applying the test-filter operator $\widehat{(\cdot)}$ to Eq. (2.3) in its entirety and subtracting the result from Eq. (3.2) gives the relationship

$$\mathcal{C}_\tau X = Y = F + P - T, \tag{3.3}$$

where is has been assumed that $\mathcal{C}_\tau$ varies slowly in space and can be removed from the test filtering operation applied to Eq. (2.3). The quantity X on the left hand side of Eq. (3.3) is given by

$$X = \hat{\overline{\rho}}\frac{Z_t}{\tau_Z^t} - \widehat{\left(\overline{\rho}\frac{Z_v}{\tau_Z}\right)}. \tag{3.4}$$

The first two terms on the right hand side of Eq. (3.3) represent the differences in convective and diffusive fluxes of variance,

$$F = \frac{\partial}{\partial x_i}\left[\widehat{\overline{\rho} Z_v \widetilde{u}_i} - \overline{\rho}(D + \widehat{D_T})\frac{\partial Z_v}{\partial x_i} - \hat{\overline{\rho}} Z_t \breve{u}_i + \hat{\overline{\rho}}(D + D_T^t)\frac{\partial Z_t}{\partial x_i}\right], \tag{3.5}$$

and in production of variance,

$$P = 2\hat{\overline{\rho}} D_T^t \frac{\partial \breve{\tilde{Z}}}{\partial x_i}\frac{\partial \breve{\tilde{Z}}}{\partial x_i} - 2\overline{\rho} D_T \widehat{\frac{\partial \widetilde{Z}}{\partial x_i}\frac{\partial \widetilde{Z}}{\partial x_i}}, \tag{3.6}$$

at the test and LES filter scales. The third term represents accumulation or loss of scalar variance between LES filter and test filter scales,

$$T = \frac{\partial \hat{\overline{\rho}} L_v}{\partial t}, \tag{3.7}$$

where L_v is the variance Leonard term,

$$L_v = Z_t - \frac{\widehat{\overline{\rho} Z_v}}{\hat{\overline{\rho}}}. \tag{3.8}$$

Since L_v can be computed directly from the resolved scalar fields, this relationship can be used to recover Z_t from Z_v.

As explained in more detail in Kaul *et al.* (2012), coefficient values are computed using a conditional least-squares method as

$$\mathcal{C}_\tau(\phi) = \frac{\langle XY | XY > 0, \phi = Z_v/\tau_Z\rangle}{\langle XX | XY > 0, \phi = Z_v/\tau_Z\rangle}, \tag{3.9}$$

where ϕ is the sample space variable corresponding to Z_v/τ_Z (Pope 2000).

4. Results of coupled DNS-LES a posteriori analysis

The dynamic nonequilibrium model was implemented in an a posteriori model evaluation framework known as the coupled DNS-LES method (Kaul & Raman 2011). In this approach, direct numerical simulation of velocity and scalar fields in homogeneous, isotropic turbulence is carried out simultaneously with the solution of transport equations for $\widetilde{Z}$ and Z_v and dynamic evaluation of the model coefficient $\mathcal{C}_\tau$. Filtered velocities from the DNS side of the simulation are used in the LES scalar equations to eliminate the influence of turbulence modeling errors, and a pseudospectral solution algorithm is used to obtain a high level of numerical accuracy.

Two sets of coupled DNS-LES computations were performed, which differed only in the specification of the LES filterwidth as either $\Delta = 8\eta$ or $\Delta = 16\eta$. The flow was characterized by a Taylor microscale Reynolds number of 135, maintained via forcing at the large scales (Alvelius 1999), and the computational mesh used 512^3 grid points.

4.1. *Domain-averaged model predictions*

The scalar fields were initialized in these simulations in an unmixed state with large regions of uniform, pure composition ($Z = 0$ or $Z = 1$). Therefore, as illustrated in Figure 1, the domain-averaged subfilter variance, $\langle Z_v \rangle$, of the scalar is initially close to zero. As the simulation proceeds, turbulent mixing increases scalar variability at progressively smaller scales and causes the average subfilter scalar variance to reach a maximum (with the magnitude of this maximum and the time at which it occurs depending on the filterwidth). Thereafter, turbulent mixing continues until molecular diffusion takes over and the scalar field very slowly relaxes towards a fully mixed state with zero subfilter variance.

In Figure 1, the modeled variance is overestimated relative to the variance values computed from the DNS scalar field for the smaller filterwidth and underestimated for the larger filterwidth. Because the domain has periodic boundary conditions in each direction, the evolution of $\langle Z_v \rangle$ is determined by the average value of the net production (production minus subfilter dissipation),

$$\frac{d\langle Z_v \rangle (t)}{dt} = \langle \mathcal{P} \rangle (t) - \langle \widetilde{\epsilon}_Z \rangle (t). \tag{4.1}$$

The domain-averaged values of production, subfilter dissipation, and net production are shown in Figures 2, 3, and 4, respectively. In each of these figures, results are given for three cases: production and dissipation computed according to their definitions from the DNS scalar field, production and dissipation computed using the subfilter modeling expressions applied to the filtered DNS scalar field (essentially performing an a priori analysis of the closures at each timestep), and LES modeled production and dissipation values. The most striking feature of these results is that the production and dissipation models generally predict values closer to the exact values taken from the DNS when applied to the LES scalar fields, rather than to the filtered DNS scalar fields. In particular, the modeled production values computed from the filtered DNS scalar field are too high, and this production overprediction is only partially offset by overprediction of the dissipation rate. Therefore, the net production predicted for the filtered DNS scalar field is also too large.

The better agreement to the exact dissipation shown by the modeled production values computed from the LES filtered scalar field, in comparison to those computed from the filtered DNS scalar field, can be explained by partial cancellation of two different modeling errors. First, the production model allows only non-negative production values, whereas

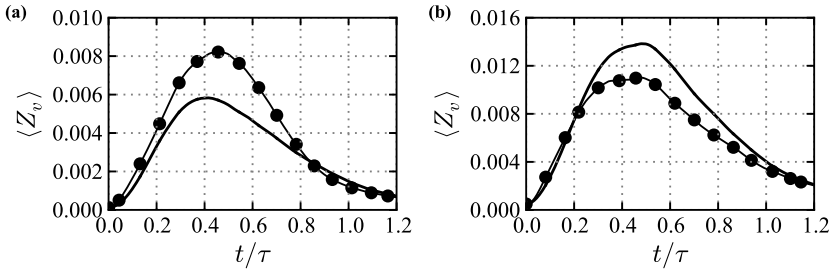

FIGURE 1. Time history of mean subfilter scalar variance for filterwidths **(a)** $\Delta/\eta = 8$ and **(b)** $\Delta/\eta = 16$. Values of Z_v are determined from (———) exact definition, Eq. (2.2), applied to DNS scalar field; (●) dynamic nonequilibrium model.

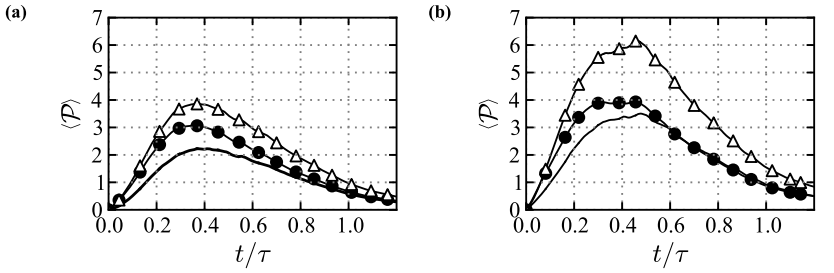

FIGURE 2. Time history of mean variance production term for filterwidths **(a)** $\Delta/\eta = 8$ and **(b)** $\Delta/\eta = 16$. Values of $\mathcal{P}$ are determined from (———) exact, unclosed form computed from DNS scalar field; (△) closed form, computed from DNS scalar field; (●) closed form, computed from the LES scalar field.

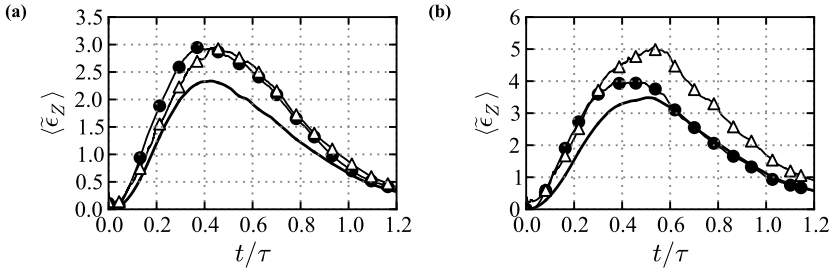

FIGURE 3. Time history of mean subfilter scalar dissipation for filterwidths **(a)** $\Delta/\eta = 8$ and **(b)** $\Delta/\eta = 16$. Values of $\tilde{\epsilon}_Z$ are determined from (———) exact definition, Eq. (2.4), applied to DNS scalar field; (△) dynamic model, computed from DNS scalar field; (●) LES implementation of the dynamic nonequilibrium model

the actual production term can take on negative values. Therefore, the model tends to overpredict production, given an appropriate estimate of the eddy diffusivity. However, the eddy diffusivity-based gradient diffusion closure of the subfilter flux term in Eq. (2.1) tends to be overdissipative, reducing the magnitude of the filtered scalar gradients and leading to lower values of production. The modeled production values computed from the filtered DNS scalar fields are affected by only the first of these two types of errors and therefore tend to be larger than those computed from the LES scalar fields.

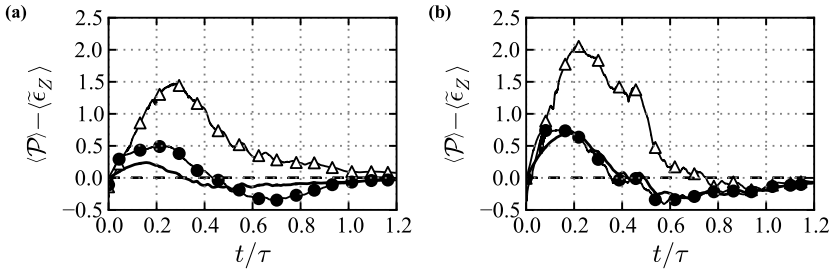

FIGURE 4. Time history of mean net production for filterwidths **(a)** $\Delta/\eta = 8$ and **(b)** $\Delta/\eta = 16$. Values of $\tilde{\epsilon}_Z$ are determined from (———) exact definitions of production and dissipation, applied to DNS scalar field; (△) dynamic model prediction computed from DNS scalar field; (●) dynamic model prediction computed from the LES scalar and variance fields.

It should be noted that the modeled production term depends only the gradients of the filtered scalar field and the modeled eddy diffusivity and therefore has a one-way relationship with the variance values predicted by the variance transport equation in a constant density flow. Clearly, an increase in the mean production leads to an increase in the predicted average subfilter variance if dissipation rate values are fixed, and, likewise, a decrease in the mean production causes a decrease in the predicted average subfilter variance under the same condition. In reality, however, the magnitude of the error induced in the predicted variance by an over- or under- estimate of production depends on the response of the dissipation rate model to the variance. The subfilter variance value appears explicitly in the dissipation rate closure, Eq. (2.5), and helps to determine the value of the model coefficient $\mathcal{C}_\tau$ taken from the conditional coefficient estimate, Eq. (3.9). Due to this nonlinearity, the effects of production rate error on dissipation rate and variance values are not obvious. In Section 5, a simplified representation of the model, based on Eq. (4.1), will be used to explore the effects of production modeling error on variance prediction. First, however, it is necessary to analyze the dynamic estimate for $\mathcal{C}_\tau$ in greater detail.

4.2. *Dynamic estimation of* $\mathcal{C}_\tau$

Because the statistics of the scalar field are not stationary in these simulations, the conditionally-evaluated coefficient values are time dependent. In this section, coefficient predictions at non-dimensional simulation times of $t = 0.2\tau$ and $t = 0.4\tau$ are examined. These times correspond to rapidly increasing and peak values of $\langle Z_v \rangle$ (see Figure 1 and were chosen with the rationale that accurate prediction of both variance and dissipation rate at later times is contingent upon their accurate prediction at earlier times.

Figure 5 compares the LES coefficient estimates to coefficient values fitted to exact variance and dissipation rate values taken from DNS data. The main point to note from this figure is that the LES dynamic model tends to predict higher coefficient values than those obtained from fitting the DNS data. An exception to this general observation occurs at the smallest values of the conditioning variable, Z_v/τ_Z, for the smaller filterwidth case [Figure 5(a)], where the LES conditional coefficient falls to a lower value. However, because Z_v/τ_Z is very small, $\tilde{\epsilon}_Z$ is also predicted to have a very low value, regardless of variations in the coefficient value of the magnitude seen here. A caveat applies to these comparisons. It must be remarked that dynamic models, by design, are meant to be responsive to the actual conditions of the filtered flow fields and, especially, to their

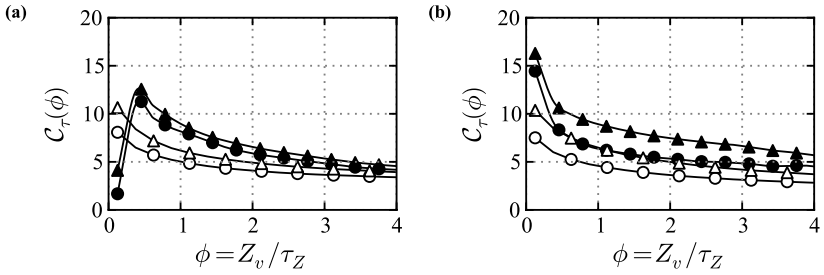

FIGURE 5. Comparison of coefficients predicted using dynamic model (Eqs. 3.3–3.7) applied to LES scalar fields and least squares fit to DNS scalar fields at filterwidths **(a)** $\Delta = 8\eta$ **(b)** $\Delta = 16\eta$. Results are shown for (●) LES dynamic model, $t = 0.2\tau$; (○) least squares fit to DNS, $t = 0.2\tau$; (▲) LES dynamic model, $t = 0.4\tau$; (△) least squares fit to DNS, $t = 0.4\tau$.

smallest resolved scales. Therefore, it would be surprising and, arguably, undesirable, for the predicted coefficients from the LES and DNS scalars to agree precisely after other statistics of the filtered DNS and LES fields have diverged. It is encouraging that the dynamic model tends to predict higher coefficient values, which helps to correct for the overprediction of variance production shown in Figure 2. Furthermore, the coefficient values predicted by the dynamic model increase from $t = 0.2\tau$ to $t = 0.4\tau$, coincident with increasing $\langle \mathcal{P} \rangle$.

Conditional means of the terms X, P, F, and T that appear in the dynamic coefficient estimate are shown for the $\Delta = 8\eta$ LES scalar fields in Figure 6. Results at $\Delta = 16\eta$ are generally similar and can be explained using similar arguments. The results shown in Figure 6 reveal an interesting pattern in how the various terms in the model combine in Eq. (3.3) to determine values of $\mathcal{C}_\tau$. The quantity F [related to variance fluxes in physical space; see Eq. (3.5)] and T [the time derivative of the variance Leonard term; see Eq. (3.7)] tend to cancel each other. Because of this, the ratio between the quantities X [related to the amount of scalar variance between the filter scales Δ and $\widehat{\Delta}$; Eq. (3.4)] and P [the difference in variance production between the two filter scales; see Eq. (3.6)] is very important in determining coefficient values

Subfilter variance production is equivalent to a transfer of variance from the resolved scales. However, the application of the variance production model at the test-filter scale is only a notional step in computing P which does not affect the evolution of the resolved scalar. Thus, changes in X and P are not necessarily in proportion. The results shown in Figure 6 suggest that the addition of variance from scales larger than $\widehat{\Delta}$ does not keep pace with the removal of variance at length scales between the filter scales $\widehat{\Delta}$ and Δ, and values of X decrease faster than those of P. Consequently, $\mathcal{C}_\tau$ increases between $t = 0.2$ and $t = 0.4$ for all values of Z_v/τ_Z, as shown in Figure 5 and discussed above.

5. Qualitative analysis of the effects of production modeling error

As discussed at the end of Section 4.1, production modeling errors have both direct and indirect effects on the evolution of subfilter variance. To qualitatively understand these effects, Eq. (4.1) can be used to construct a simplified representation of the variance evolution under the dynamic nonequilibrium model, or in other words, to "model the model."

To numerically integrate Eq. (4.1) under the effects of various levels of production

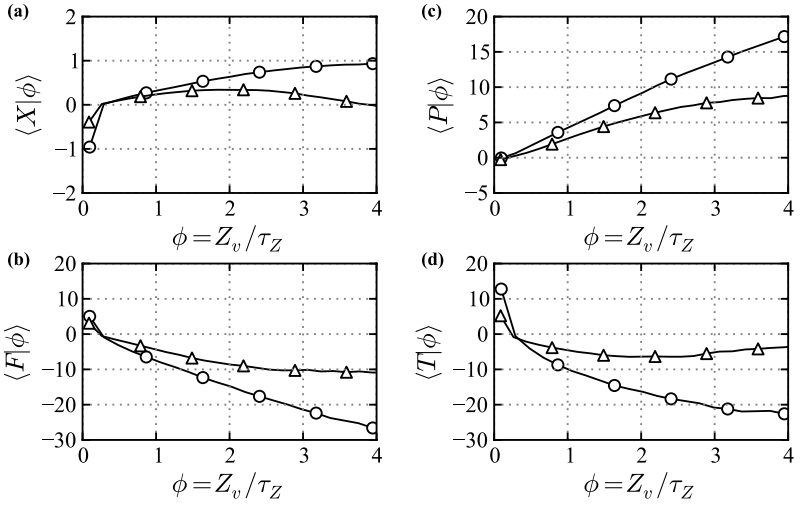

FIGURE 6. Conditional means of quantities in the dynamic model computed from LES scalar fields **(a)** X, Eq. (3.4) **(b)** F, Eq. (3.5) **(c)** P, Eq. (3.6) **(d)** T, Eq. (3.7). Simulation times shown are (○) $t = 0.2\tau$, (△) $t = 0.4\tau$.

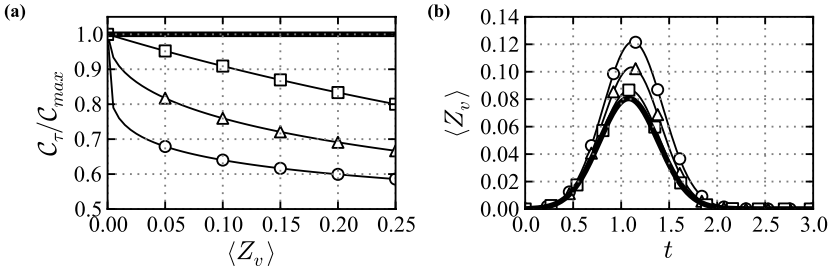

FIGURE 7. **(a)** Coefficient variation with mean variance in Eq. (5.1) **(b)** Time history of mean variance computed using Eq. (4.1). Dissipation model exponent values are (○) $k = 1/4$, (□) $k = 1/2$, (△) $k = 1$, (———) $k = \infty$.

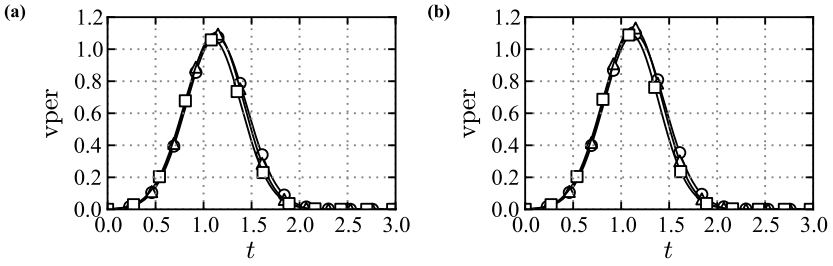

FIGURE 8. Ratios of variance and production error, vper, for $\mathcal{C}_{max} = \mathcal{C}_{max,0}$ and **(a)** $\mathcal{P}_{max} = 4/5\mathcal{P}_{max,0}$ **(b)** $\mathcal{P}_{max} = 6/5\mathcal{P}_{max,0}$. Values of k shown are (○) $k = 1/4$, (□) $k = 1/2$, (△) $k = 1$, (———) $k = \infty$.

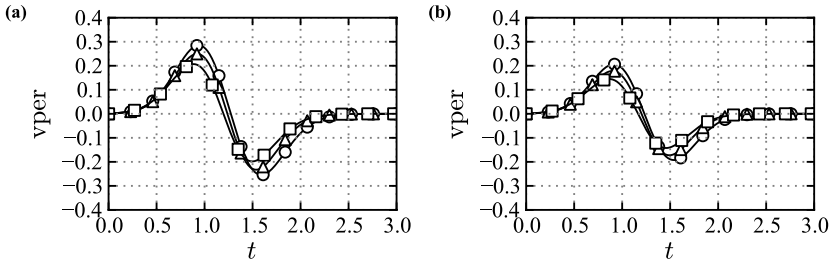

FIGURE 9. Ratios of variance and production error, vper, for $\mathcal{C}_{max}$ linearly proportional to $\mathcal{P}_{max}$ and **(a)** $\mathcal{P}_{max} = 4/5\mathcal{P}_{max,0}$ **(b)** $\mathcal{P}_{max} = 6/5\mathcal{P}_{max,0}$. Values of k shown are (○) $k = 1/4$, (□) $k = 1/2$, (△) $k = 1$, (———) $k = \infty$.

modeling error, analytical expressions for mean production and mean dissipation are required. The mean production is supplied by a prescribed bell-shaped curve whose shape is characteristic of the mean production evolution shown in Figure 2. To represent systematic under- or overprediction of production, a premultiplying factor $\mathcal{P}_{max}$ is set to values of 4/5 and 6/5 times a baseline value $\mathcal{P}_{max,0}$. This twenty percent error was chosen as comparable to the error observed in the LES results. For this flow field, it was found that the mixing timescale, τ_Z, has a low level of correlation with Z_v and the two quantities are be approximated as uncorrelated. Additionally, since τ_Z depends primarily on the velocity fields, which are statistically stationary, $\langle \tau_Z \rangle$ is treated as a constant.

To emulate the nonlinear relationship between variance and dissipation rate that is allowed by the full LES dynamic model for $\mathcal{C}_\tau$, the mean dissipation in Eq. (4.1) is determined by

$$\langle \widetilde{\epsilon}_Z \rangle = \mathcal{C}_\tau(\langle Z_v \rangle) \frac{\langle Z_v \rangle}{\langle \tau_Z \rangle} = \frac{\mathcal{C}_{max}}{1 + \langle Z_v \rangle^k} \frac{\langle Z_v \rangle}{\langle \tau_Z \rangle} \tag{5.1}$$

where $\mathcal{C}_{max}$ is the maximum value of the dissipation rate model constant. In the first set of calculations to be discussed, $\mathcal{C}_{max}$ has a fixed value, $\mathcal{C}_{max,0}$, regardless of the value of $\mathcal{P}_{max}$. In the second set of calculations, $\mathcal{C}_{max}$ varies linearly with $\mathcal{P}_{max}$. The exponent k in Eq. (5.1) is set to values of 1/4, 1/2, 1, and ∞ (the constant coefficient case). Thus, as shown in Figure 7(a) the coefficient value holds steady or decreases as $\langle Z_v \rangle$ increases, consistent with the coefficient variation usually found in the coupled DNS-LES simulations. The variation of $\mathcal{C}_\tau$ versus $\langle Z_v \rangle$ with these choices of k is illustrated in Figure 7(a). With these parameterization choices, the mean variance evolutions under Eq. (4.1) can be identified by the prescribed values of $\mathcal{P}_{max}$ and k. Sample variance time histories for baseline values $\mathcal{P}_{max} = \mathcal{P}_{max,0}$, $\mathcal{C}_{max} = \mathcal{C}_{max,0}$ are shown in Figure 7(b). As an obvious consequence of Eq. (5.1), $\langle Z_v \rangle$ increases as k decreases.

A quantity called the variance-to-production error ratio, abbreviated as vper, is defined here to discuss the results,

$$\text{vper} = \left[\frac{\langle Z_v \rangle_{\mathcal{P}_{max},k} - \langle Z_v \rangle_{\mathcal{P}_{max,0},k}}{\max\left(\langle Z_v \rangle_{\mathcal{P}_{max,0},k} \right)} \right] \left[\frac{\mathcal{P}_{max} - \mathcal{P}_{max,0}}{\mathcal{P}_{max}} \right]^{-1} \tag{5.2}$$

As its name implies, vper is the ratio between the relative error in variance induced by an error in production (first bracketed quantity) to the relative error in production (second

bracketed quantity), for a given value of k in the dissipation rate expression, Eq. (5.1). In the constant coefficient case, the peak value of vper is unity.

First, the direct effect of production modeling error is assessed by setting $\mathcal{C}_{max} = \mathcal{C}_{max,0}$ for all three values of $\mathcal{P}_{max}$. Values of vper obtained from these calculations for under- and overprediction of production are shown in Figures 8(a) and (b), respectively. In both cases, the variation of $\mathcal{C}_\tau$ with $\langle Z_v \rangle$ magnifies the effect of the production error. If production is underpredicted, $\langle Z_v \rangle$ shifts to a lower value, increasing $\mathcal{C}_\tau$. This increases the dissipation and further decreases $\langle Z_v \rangle$. Conversely, if production is overpredicted, $\langle Z_v \rangle$ shifts to a higher value, decreasing $\mathcal{C}_\tau$. This decreases the dissipation and further increases $\langle Z_v \rangle$. Interestingly, values of vper are about the same for all three values of k. Figure 7 explains this finding. Except for very low values of $\langle Z_v \rangle$, which occur only briefly, the slope $d\mathcal{C}_\tau / d\langle Z_v \rangle$ does not depend strongly on k.

Next, direct and indirect effects of production error are combined by making $\mathcal{C}_{max}$ dependent on $\mathcal{P}_{max}$. Based on the results presented in Section 4.2, an increase in $\mathcal{P}_{max}$ is assumed to increase $\mathcal{C}_{max}$. For simplicity, a linear relationship is used: $\mathcal{C}_{max}/\mathcal{C}_{max,0} = \mathcal{P}_{max}/\mathcal{P}_{max,0}$. Figure 9 shows values of vper obtained in these computations. The change in $\mathcal{C}_{max}$ at first partially compensates for, and later overcompensates for, the change in $\mathcal{P}_{max}$. This is shown by the decrease in peak vper and the fact that vper changes sign, passing from positive to negative values around $t = 1$, or about the same time variance values reach their peak. Thus, the response of the model coefficient to the production error decreases the effect of the production error on the variance prediction. However, the sign of the variance error can be counterintuitive, with overprediction of production eventually inducing an underprediction of variance, and vice versa.

6. Summary and conclusions

This work presented a detailed analysis of a recently introduced dynamic nonequilibrium modeling approach for subfilter scalar dissipation rate and subfilter scalar variance (Kaul *et al.* 2012). This modeling approach is composed of three sub-models: the variance transport equation, a mixing timescale-based model for dissipation rate, and the novel element, a dynamic estimation procedure for the model coefficient $\mathcal{C}_\tau$. Each of these sub-models makes different assumptions and can introduce different types of errors that affect the predicted values of Z_v and $\widetilde{\epsilon}_Z$, and therefore each needs to be evaluated for accuracy. However, the sub-models are closely interdependent and this interdependence is actually an essential feature of the overall modeling approach that allows the formulation of the dynamic procedure of $\mathcal{C}_\tau$ in the first place. A single analysis method is not sufficient for such a multifaceted analysis task. Instead, a hierarchy of methods is needed. Following on the turbulent, lifted flame simulations presented in Kaul *et al.* (2012), this work used two techniques with progressively greater simplification or abstraction of the problem.

First, a technique for a posteriori analysis of scalar models called the coupled DNS-LES method was used to evaluate the performance of the dynamic nonequilibrium model in homogeneous, isotropic turbulence apart from numerical and turbulence modeling errors. Errors in variance prediction were found to depend on the extent to which errors in modeling production and dissipation of variance cancelled each other. Furthermore, it was noted that production modeling errors have both a direct and indirect effect on variance prediction, where the indirect effect occurs through the dynamic prediction of $\mathcal{C}_\tau$. Closer examination of the terms in the coefficient estimation procedure indicated that an increase in production tends to increase $\mathcal{C}_\tau$. Next, a "model of the model" in the form of an

ordinary differential equation describing the evolution of the mean subfilter variance was used to qualitatively examine the effects of production modeling error. It was found that dynamic estimation of $\mathcal{C}_\tau$ can lead to counterintuitive results, such as underprediction of production causing overprediction of variance, and vice versa. Encouragingly, however, these results suggested that dynamic computation of $\mathcal{C}_\tau$ can effectively compensate for production modeling error, yielding more accurate predictions of variance.

REFERENCES

Alvelius, K. 1999 Random forcing of three-dimensional homogeneous turbulence. *Phys. Fluids* **11** (7), 1880–1889.

Balarac, G., Pitsch, H. & Raman, V. 2008 Development of a dynamic model for the subfilter scalar variance using the concept of optimal estimators. *Phys. Fluids* **20**, 035114.

da Silva, C. B. & Pereira, J. C. F. 2005 On the local equilibrium of the subgrid scales: The velocity and scalar fields. *Phys. Fluids* **17**, 108103.

Germano, M., Piomelli, U., Moin, P. & Cabot, W. H. 1991 A dynamic subgrid-scale eddy viscosity model. *Phys. Fluids* **7**, 1760–1765.

Ghosal, S., Lund, T. S., Moin, P. & Akselvoll, K. 1995 A dynamic localization model for large-eddy simulation of turbulent flows. *J. Fluid Mech.* **286**, 229–255.

Jimenez, C., Ducros, F., Cuenot, B. & Bedat, B. 2001 Subgrid scale variance and dissipation of a scalar field in large eddy simulations. *Phys. Fluids* **13**, 1748.

Kaul, C. M. & Raman, V. 2011 A posteriori analysis of numerical errors in subfilter scalar variance modeling for large eddy simulation. *Phys. Fluids* **23** (3), 035102.

Kaul, C. M., Raman, V., Balarac, G. & Pitsch, H. 2009 Numerical errors in the computation of subfilter scalar variance in large eddy simulations. *Phys. Fluids* **21**, 055102.

Kaul, C. M., Raman, V., Knudsen, E., Richardson, E. S. & Chen, J. H. 2012 Large eddy simulation of a lifted ethylene flame using a dynamic nonequilibrium model for subfilter scalar variance and dissipation rate. *Proc. Comb. Inst.* **In press.**

Knudsen, E., Richardson, E. S., Doran, E. M., Pitsch, H. & Chen, J. H. 2012 Modeling scalar dissipation and scalar variance in large eddy simulation: Algebraic and transport equation closures. *Phys. Fluids* **24**, 055103.

Moin, P., Squires, K., Cabot, W. & Lee, S. 1991 A dynamic subgrid-scale model for compressible turbulence and scalar transport. *Phys. Fluids A* **3**, 2746–2757.

Peters, N. 2000 *Turbulent Combustion*. Cambridge University Press.

Pierce, C. D. & Moin, P. 1998 A dynamic model for subgrid-scale variance and dissipation rate of a conserved scalar. *Phys. Fluids* **10**, 3041–3044.

Pitsch, H. 2006 Large-eddy simulation of turbulent combustion. *Ann. Rev. Fluid Mech.* **38**, 453–482.

Pope, S. B. 2000 *Turbulent Flows*. Cambridge University Press.

Raman, V. & Pitsch, H. 2006 A consistent LES/filtered-density function formulation for the simulation of turbulent flames with detailed chemistry. *Proc. Comb. Inst.* **31**, 1711–1719.